Control over phase behavior and solution structure of hairy-rod polyfluorene by means of side-chain length and branching

M. Knaapila,[1,2,*] R. Stepanyan,[3] M. Torkkeli,[4] V. M. Garamus,[5] F. Galbrecht,[6] B. S. Nehls,[6,7] E. Preis,[6] U. Scherf,[6] and A. P. Monkman[8]

[1]*Department of Physics, Institute for Energy Technology, P.O. Box 40, NO-2027 Kjeller, Norway*

[2]*MAX-lab, Lund University, P.O. Box 118, SE-22100 Lund, Sweden*

[3]*Materials Science Centre, DSM Research, P.O. Box 18, NL-6160 MD Geleen, The Netherlands*

[4]*Department of Physics, P.O. Box 64, FI-00014 University of Helsinki, Finland*

[5]*GKSS Research Centre, Max-Planck-Strasse 1, DE-21502 Geesthacht, Germany*

[6]*Fachbereich Chemie, Bergische Universität Wuppertal, Gauß-Strasse 20, DE-42097 Wuppertal, Germany*

[7]*BASF-SE, Global Polymer Research, GKT/F, DE-67056 Ludwigshafen, Germany*

[8]*Department of Physics, University of Durham, South Road, DH1 3LE Durham, United Kingdom*

(Received 6 February 2008; published 8 May 2008)

We present guidelines on how the solution structure of π-conjugated hairy-rod polyfluorenes is controlled by the side-chain length and branching. First, the semiquantitative mean-field theory is formulated to predict the phase behavior of the system as a function of side-chain beads (N). The phase transition at $N=N^*$ separates a lyotropic phase with solvent coexistence ($N<N^*$) and a metastable membrane phase ($N>N^*$). The membrane phase transforms into the isotropic phase of dissolved rodlike polymers at the temperature $T^*_{\mathrm{mem}}(N)$, which decreases both with N and with the degree of side-chain branching. This picture is complemented by polymer demixing with the transition temperature $T^*_{IN}(N)$, which decreases with N. For $N<N^*$, the lyotropic phase turns isotropic with increasing T at T^*_{IN}. For $N>N^*$, stable membranes are predicted for $T^*_{IN}<T<T^*_{\mathrm{mem}}$ and metastable membranes with nematic coexistence for $T<T^*_{IN}$. Second, in experiment, samples of poly(9,9-dialkylfluorene) with $N=6-10$ were mixed in methylcyclohexane. For $N=8$ the side-chain branching was controlled by (9,9-dioctylfluorene)/(9,9-bis(2-ethylhexyl)fluorene) (F8/F2/6) random copolymers. The proportion of F8 to F2/6 repeat units was 100:0, 95:5, 90:10, 50:50, and 0:100. In accordance with the theory, lyotropic, membrane, and isotropic phases with the corresponding phase transitions were observed. For $N<N^*\sim 6$ only the lyotropic phase is present for attainable temperatures. The membrane and isotropic phases are present for $N>N^*$. $T^*_{\mathrm{mem}}(N)$ decreases from 340 K to 280 K for $N\geq 8$. For copolymers, the membrane phase is found when the fraction of F8 units is at least 90%, T^*_{mem} decreasing with this fraction. The membrane phase contains three material types: loose sheets of two polymer layers, a better packed β phase, and dissolved polymer. For $N\geq 7$ and $T<T^*_{\mathrm{mem}}$ the tendency for membrane formation becomes stronger with increasing temperature.

DOI: 10.1103/PhysRevE.77.051803 PACS number(s): 36.20.−r, 81.16.Dn, 82.35.Lr, 64.60.Cn

I. INTRODUCTION

Understanding of intermolecular self-organization [1,2] is critical in the materials science of hairy-rod polymers [3]. An important class of self-assembling hairy rods is composed of π-conjugated polymers [4] among which polyfluorenes (PFs) [5–8] are employed in myriad applications in solution-processed polymer electronics [9]. The phase behavior of PFs has been extensively studied in the solid state, but the literature of their solution assemblies remains not all inclusive, specific exceptions including systems such as poly(9,9-dioctylfluorene) (PF8) [10–14], poly(9,9-bis(2-ethylhexyl)fluorene) (PF2/6) [13,15,16], (2-ethylhexyl)fluorene oligomers (F2/6) [17], poly(9,9-dialkylfluorene-*co*-fluorenone) copolymers [18], and poly(9,9-bis((*S*) -3,7-dimethyloctyl))fluorene) [19]. More systematic studies of the various aspects of solution assemblies would yet be advantageous not least because the solvent plays a role in the morphology of the solvent-processed thin films [20] and nano-objects [21].

The theoretical phase behavior of hairy-rod solutions has been addressed by Ballauff [22] in a framework of a Flory lattice model. It has been shown that an isotropic solution of hairy rods is stable only in a low-concentration and high-temperature regime. Upon decreasing the temperature the system phase separates into virtually pure solvent and lyotropic nematic with relatively high polymer concentration. The isotropic-nematic liquid transition temperature (T^*_{IN}) decreases as a function of the side-chain length, hence longer side chains postponing demixing. However, the formation of any intermediate (possibly metastable) membrane structure has been left out of this picture. Therefore, there is an interest in metastable membrane structures of hairy-rod polymers.

Phenomenologically, the solution behavior of PFs can be rationalized in terms of three experimental variables: the nature of solvents, fraction of polymers, and nature of side chains. The length of the polymer is another parameter becoming dominant for oligomers [17]. A major structural diversity arises from the quality of the solvent, the first parameter. For example, PF8 forms sheetlike particles in 1 wt % solution of a poor solvent methylcyclohexane (MCH) and an isotropic phase of rodlike polymers in a better solvent, toluene [13]. Alternatively, if the polymer fraction, the second

*Author to whom correspondence should be addressed: FAX: +47-6381-0920. matti.knaapila@ife.no

parameter, is increased from 1 wt % to 3–7 wt % in toluene, stiff PF8 molecules turn to a large networklike structure [23].

In our previous work [13,14] we studied the nature of the side-chain length, the third variable, using branched side-chain PF2/6 and a series of linear side-chain PFs—poly(9,9-dihexylfluorene) (PF6), poly(9,9-diheptylfluorene) (PF7), PF8, poly(9,9-dinonylfluorene) (PF9), and poly(9,9-didecylfluorene) (PF10)—in MCH. In MCH, PF6, PF7, PF8, and PF9 form sheetlike particles whereas PF2/6 and PF10 remain fully dissolved rodlike chains. In this work the experiments were performed at 20 °C and full thermal characterization would significantly complement the results.

The photophysics of the so-called β phase is another motivation for our phase behavioral investigations. The β phase [24] is well known for solid-state PF8, which is polymorphic with a range of crystalline [25] and noncrystalline [26] phases. These phases originate from classes of conformational isomers (denoted as C_α, C_β, etc.), defined by the torsional angle between repeat units [27,28]. The β phase is a solid-state manifestation of the single isomer C_β with a torsional angle of around 160°–165°. The β phase is extraordinary among π-conjugated polymers with very narrow linewidths in its optical spectra [29], showing even potency in lasing [30]. As MCH mixtures of PF7, PF8, and PF9 contain a large amount of the nearly planar conformational isomer C_β [10,14], the question remains whether its fraction could be controlled by nanoscale solution assemblies.

The objectives of the present paper are thus as follows. First, we aim at connecting the formation of two-dimensional structures (or membranes) to the experimental framework of PFs as a function of side-chain length, N denoting the number of side-chains beads. Particular attention is placed on the membrane structures. Instead of focusing on room temperature, we probe a fully accessible temperature range. Second, we keep N constant and vary the degree of side-chain branching by means of copolymerization. When the theoretical and experimental results are merged, we find that the lyotropic phase and the metastable (and potentially stable) membrane phase exist in PF solution with increasing N. The lyotropic-membrane phase transition is observed at $N^* \sim 6$. The membrane phase turns to the isotropic phase of dissolved rodlike polymers at $T^*_{\mathrm{mem}}(N=7-10)$, this value sharply decreasing for $N \geq 8$. The degree of side-chain branching decreases T^*_{mem}. The membrane phase is present when the fraction of linear chain monomers is at least 90%. The details of the polymer demixing and the components of membrane phase are moreover given. The β phase with lateral order exists in the membrane phase regime alongside with loose membranes. The tendency for membrane formation becomes more prominent just below T^*_{mem}.

Teetsov and Vanden Bout [31] demonstrated how the surface morphology of PFs can be varied by the side-chain length in thin films. In this paper we show in turn how their structure can be controlled by the side-chain length and branching in solution. Overall, we have hitherto shown that PFs provide a versatile theoretical and experimental tool to study the phase behavior of hairy rods in the solid state and thin films [6]. In this paper we show that PFs constitute also a model system for solution studies. The concepts presented may be applied to other π-conjugated hairy-rod solutions with isotropic and membrane phases. A phenomenologic connection is seen, for example, to the solutions of poly-2-methoxy-5-(2'-ethyl-hexyloxy)-1,4-phenylene vinylene (MEH-PPV) [32].

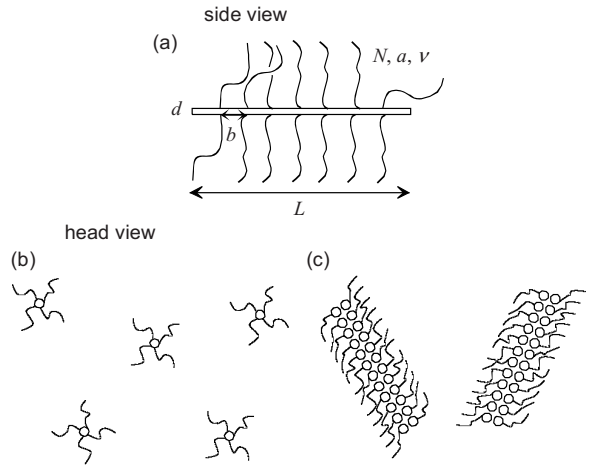

FIG. 1. (a) A hairy-rod molecule. N, a, and ν are, respectively, the number of side-chain beads as well as its statistical length and excluded volume, while b, d, and L are, respectively, the grafting distance, diameter, and length of the backbone. (b) Solution of noninteracting hairy rods. (c) Solution of hairy-rod membranes. Here a simplified two-dimensional picture is drawn with the rods parallel (a) or perpendicular (b) and (c) to the drawing plane.

II. THEORY

A. Free energies

In a simplified way, a hairy-rod molecule is understood as a rigid cylinder with flexible side chains attached to it [cf. Fig. 1(a)]. Although the backbone-solvent interaction favors demixing, the hairy-rods can be dissolved to form a dilute solution of noninteracting molecules at high temperatures [Fig. 1(b)]. Such a system ultimately demixes on cooling. Furthermore, as will be shown in the experimental part of the work, intermediate structures or "membranes" [Fig. 1(c)] can appear on the way from the solution to the ultimate demixed state. The scaling behavior of the solution-membrane transition temperature as a function of the side-chains length can be estimated by comparing the free energies of both phases as follows. In order to make this estimation we start with the free energy of the isotropic solution phase which reads as

$$F^{(\mathrm{sol})} = F^{(\mathrm{sol})}_{\mathrm{brush}} + F^{(\mathrm{sol})}_{RS} + F^{(\mathrm{sol})}_{RA} + F^{(\mathrm{sol})}_{\mathrm{tr}}, \tag{1}$$

where the brush term $F^{(\mathrm{sol})}_{\mathrm{brush}}$ includes the excluded-volume interaction between the alkyl chains in a good solvent and their stretch (which has been calculated, e.g., in Ref. [33]). Per side chain this contribution reads as

$$F^{(\mathrm{sol})}_1 = k_B T \left(\frac{\nu N}{a^2 b} \right)^{1/2}, \tag{2}$$

where ν is the excluded volume of a side-chain monomer in

a good solvent and N and a the number of side-chain beads (units per side chain) and its statistical segment length, respectively. Here b is the grafting distance along the backbone. The next two terms $F_{RS}^{(\mathrm{sol})}$ and $F_{RA}^{(\mathrm{sol})}$ represent the interaction of the backbone rod (R) with solvent (S) molecules and alkyl chains (A), respectively. Finally, the last term incorporates the translational free energy of the hairy-rod molecules.

In order to proceed the approach developed in Refs. [34,35] is employed to estimate the rod-solvent interaction free energy as

$$\frac{F_{RS}^{(\mathrm{sol})}}{N_{\mathrm{tot}}} = 2Ld\gamma_{RA}\nu_0 c^{(\mathrm{sol})}, \tag{3}$$

where the "interfacial" energy parameter γ_{RS} describes the interaction between backbone and solvent [34]. L and d are the length and diameter of the stiff backbone, N_{tot} the total number of molecules in the system, ν_0 the monomeric volume, and $c^{(\mathrm{sol})}$ the concentration of the solvent molecules in the vicinity of the backbone. Using the same arguments we get

$$\frac{F_{RA}^{(\mathrm{sol})}}{N_{\mathrm{tot}}} = 2Ld\gamma_{RA}\nu_0 c_2, \tag{4}$$

where c_2 is the concentration of the alkyl monomers around the backbone so that $\nu_0(c_2^{(\mathrm{sol})}+c_2)\equiv 1$. In the formulas above some constants of the order of unity are omitted. The last term in Eq. (1) accounts for the translational entropy which has the same form as in the Flory type theories:

$$F_{\mathrm{tr}}^{(\mathrm{sol})} = k_B T N_{\mathrm{tot}}\left[\ln\frac{f}{e} + \frac{1-f}{\nu_0 f}\left(\frac{\pi d^2 L}{4} + \frac{\nu_0 NL}{b}\right)\ln\frac{1-f}{e}\right], \tag{5}$$

where f is the volume fraction of the polymer in the system. Finally, the free energy of the isotropic solution phase, Eq. (1), takes the form

$$\frac{F^{(\mathrm{sol})}}{N_{\mathrm{tot}}k_B T} = \frac{L}{b}\left(\frac{\nu N}{a^2 b}\right)^{1/2} + 2Ld\left[\frac{\gamma_{RS}}{k_B T}(1-\nu_0 c_2) + \frac{\gamma_{RA}}{k_B T}\nu_0 c_2\right] + \ln\frac{f}{e} + \frac{1-f}{\nu_0 f}\left(\frac{\pi d^2 L}{4} + \frac{\nu_0 NL}{b}\right)\ln\frac{1-f}{e}, \tag{6}$$

with $c_2=(a^2b^2d^2\nu)^{-1/3}$ calculated based on the formulas given in Ref. [33].

The free energy of the other competing phase, the solution with membranes, can be calculated along the same lines, which yields

$$\frac{F^{(\mathrm{mem})}}{N_{\mathrm{tot}}k_B T} = \frac{2NL}{b}\left(\frac{\nu}{abd}\right)^{2/3} + Ld\left[\frac{\gamma_{RS}}{k_B T}(1-\nu_0 c_1) + \frac{\gamma_{RA}}{k_B T}\nu_0 c_1\right] + \frac{1-f}{\nu_0 f}\left(\frac{\pi d^2 L}{4} + \frac{\nu_0 NL}{b}\right)\ln\frac{1-f}{e}, \tag{7}$$

where $c_1=\nu^{-1/3}(abd)^{-2/3}$ is the concentration of the alkyl monomers around a double-layered sheet of backbones. We also made use of $F_1^{(\mathrm{mem})}=2k_B N(\nu/abd)^{2/3}$ for the planar brush free energy per chain [36]. The interaction free energy is corrected by the fact that only a half of the surface area of the rods is in contact with solvent or side chains.

B. Membrane-isotropic transition

The free energies lead to an estimation of the membrane-isotropic solution transition temperature T_{mem}^*. By equating Eqs. (6) and (7) we get

$$\frac{1}{k_B T_{\mathrm{mem}}^*} = \frac{2(\nu/abd)^{2/3}N - (\nu/a^2 b)^{1/2}\sqrt{N} - (b/L)\ln(f/e)}{bd[\gamma_{RS} + (\gamma_{RA}-\gamma_{RS})\nu_0(2c_2-c_1)]}. \tag{8}$$

Here we assume that ν, γ_{RA}, and γ_{RS} do not depend on the temperature. Although generally incorrect, these assumptions do not change the scaling behavior of T_{mem}^*. Another important point is that the Eq. (8) is valid for relatively long side chains, at least as long as the distance between their grafting points is smaller than their Flory radius $R_F = a(\nu/a^3)^{1/5}N^{3/5}$—i.e., $N>N^*=(b/a)^{5/3}(\upsilon/a^3)^{1/3}$. For shorter side chains one can expect a picture where the isotropic liquid demixes with decreasing temperature [22].

C. Polymer-solvent demixing

We have so far ignored polymer-solvent demixing. Without addressing it in detail we note that for long enough side chains demixing can give rise to a highly concentrated, almost a melt, phase (with lamellar morphology) and virtually pure solvent. The free energy after demixing is of the order of

$$\frac{F^{(\mathrm{demix})}}{N_{\mathrm{tot}}k_B T} = \frac{3NL}{2b}\left(\frac{\nu}{abd}\right)^2 + Ld\frac{\gamma_{RA}}{k_B T}, \tag{9}$$

where $F_1^{(\mathrm{lam})}=3/2k_B TN[\nu_0/(abd)]^2$ is the elastic energy per side chain (see Ref. [34] for details). The free energy of demixing, Eq. (9), scales as the one of the membrane phase, Eq. (7), which might imply that either the regime of thermodynamic stability of membranes is quite narrow or it is thermodynamically unstable. Accordingly, the demixing temperature T_{IN}^* with

$$\frac{1}{k_B T_{IN}^*} = \frac{\frac{3}{2}\left(\frac{\nu}{bad}\right)^2 N - \left(\frac{\nu}{a^2 b}\right)^{1/2}\sqrt{N} - \frac{b}{L}\left[\ln\frac{f}{e} + \frac{1-f}{\nu_0 f}\left(\frac{\pi d^2 L}{4} + \frac{\nu_0 NL}{b}\right)\ln\frac{1-f}{e}\right]}{bd[\gamma_{RS} + (\gamma_{RA}-\gamma_{RS})(1-\nu_0 c_2)]} \tag{10}$$

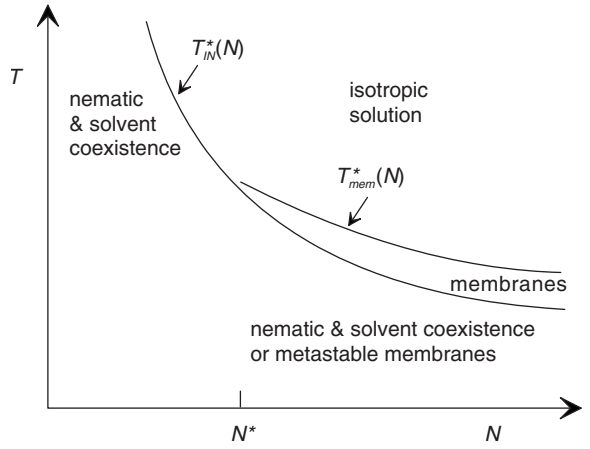

FIG. 2. The schematic presentation of transition temperatures $T^*_{IN}(N)$ and $T^*_{\mathrm{mem}}(N)$ of a hairy-rod solution as a function of side-chain length. N is the number of side-chain beads. For long side chains, membranes can appear as an intermediate step between the isotropic solution and demixed state. The demixing temperature $T^*_{IN}(N)$, here shown schematically, has been calculated in Ref. [22].

is expected to be close to the membrane-isotropic transition temperature T^*_{mem}.

D. Phase diagram

Overall, the membrane-isotropic and isotropic-nematic phase transition temperatures are predicted by Eqs. (8) and (10). These results are qualitatively sketched in Fig. 2.

III. EXPERIMENT

A. Materials

The chemical structures of the PFs used are shown in Fig. 3. PF6, with number-averaged molecular weight (M_n)=84 kg/mol and the weight-averaged molecular weight (M_w)= 200 kg/mol), PF7 (M_n=63 kg/mol, M_w =144 kg/mol), poly(9,9-dioctylfluorene), PF8 (M_n =48 kg/mol, M_w=132 kg/mol), PF9 (M_n=109 kg/mol, M_w=221 kg/mol), and PF10 (M_n=86 kg/mol, M_w =236 kg/mol) were prepared following the Yamamoto-type polycondensation of the corresponding 2,7-dibromo-9,9-dialkylfluorenes with Ni(COD)$_2$ [8]. In this case (9,9-dioctylfluorene)/(9,9-bis(2-ethylhexyl)fluorene) random copolymers (or F8-F2/6) ($M_n \gg 5$ kg/mol) and poly(9,9-bis(2-ethylhexyl)fluorene)/(9-fluorenone) random copolymer (or F2/6-fluorenone) were prepared starting from the mixtures of the corresponding 2,7-dibromo-9,9-dialkylfluorene/2,7-dibromo-9-fluorenone monomers [37]. The applied molar ratios of 9,9-dialkylfluorene (F8) to 9,9-bis(2-ethylhexyl)fluorene (F2/6) repeat units were 95:5 (the corresponding polymer is denoted as $F8_{0.95}$-$F2/6_{0.05}$), 90:10 ($F8_{0.90}$-$F2/6_{0.10}$), and 50:50 ($F8_{0.50}$-$F2/6_{0.50}$). For the F2/6-fluorenone copolymer the molar ratio of the proportion of 9,9-bis(2-ethylhexyl)fluorene to 9-fluorenone repeat units was 95:5 (the polymer is denoted as $F2/6_{0.95}$-$\mathrm{fluorenone}_{0.05}$).

The PFs were dissolved in either 10 mg/ml MCH (Sigma-Aldrich) or deuterated methylcyclohexane (MCH-d_{14})

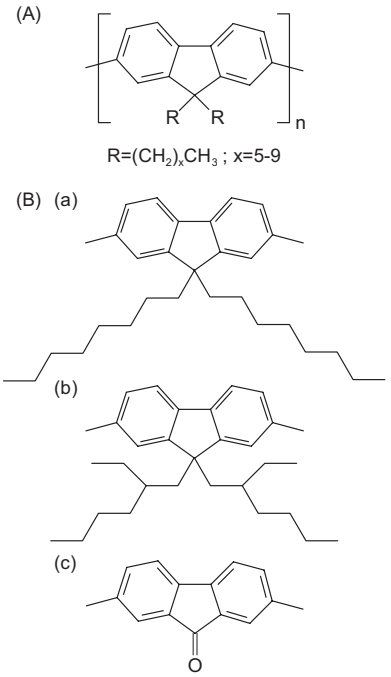

FIG. 3. (a) Chemical structures of PFs studied as a function of the side-chain length. (b) Chemical structure of random copolymers constituting different degree of side-chain branching. In this case F8 [(a)] and F2/6 monomers [(b)] were mixed with molar ratios of 95:5, 90:10, and 50:50. Additionally F2/6 (b) was mixed with 9,9-bis-fluorenone units [(c)] with a ratio of 90:10.

(99.5% D, Apollo Scientific Ltd). MCH-d_{14} was employed in the case of neutron scattering, whereas MCH was used otherwise. Only PF10 is soluble in MCH at room temperature at the applied concentration. To achieve a complete solution at the elevated temperature and subsequent gelation [13,14] at low temperature, the mixtures were prepared via a heating-cooling cycle. In a typical procedure the mixtures were first heated up to 80–85 °C and stirred for 5–10 min until completely clear solutions were observed. These samples were then cooled from 80–85 °C down to −25 °C for 30 min and subsequently warmed to 20 °C before measurements. In this procedure the PF6/MCH, PF7/MCH, PF8/MCH, PF9/MCH, $F8_{0.95}$-$F2/6_{0.05}$/MCH, and $F8_{0.90}$-$F2/6_{0.10}$/MCH mixtures become viscous or gel-like at 20 °C while other mixtures appear as transparent liquids. PF6 is an exception, and due to the poorer solubility, the mixture was typically heated up to 100 °C, a temperature limited by the boiling point of MCH (101 °C). However, PF6/MCH is not transparent even at 100 °C.

B. Small-angle neutron scattering

Small-angle neutron scattering (SANS) was employed for structural studies. For neutron scattering, the solutions were prepared via a heating-cooling cycle described above. The SANS measurements were made immediately after sample preparation at two constant temperatures. No significant macrophase separation was observed during the measurements (over a few hours).

SANS measurements were performed using the SANS-1 instrument at the GKSS Research Centre in Geesthacht, Germany [38]. Several sample-to-detector distances (from 0.7 to 9.7 m) and wavelength 8.1 Å were employed to cover the q range from 0.004 to 0.3 $Å^{-1}$. The samples were filled in Hellma quartz cells of 2 mm path length. The temperature was controlled by a Julabo thermostat. The raw scattering patterns were corrected for sample transmission and air sample cell scattering by conventional procedures [39]. The isotropic two-dimensional scattering patterns were azimuthally averaged, converted to an absolute scale and corrected for detector efficiency dividing by the incoherent scattering spectra of 1-mm-thick pure water. The scattering from MCH-d_{14} used for the sample preparation was subtracted as a background. The small incoherent scattering due to the nondeuterated polymer was taken into account in the fitting procedures (see Sec. IV).

C. Small-angle and wide-angle x-ray scattering

Small- and wide-angle x-ray scattering (SAXS and WAXS) were used to monitor the thermal process *in situ*. The samples were prepared following the above-mentioned procedure by dissolving in MCH on a hot plate. Then, the mixtures were transferred with a syringe rapidly to the preheated sample holders, sealed with epoxy, and measured at 80 °C for 15 min to check whether they are dissolved to the molecular level. Thereafter they were quenched in approximately 1 min to −12 °C, measured (and kept) there for 30 min, and heated slowly (0.1 °C/min) back to 80 °C while measuring. An exception was PF10/MCH which was dissolved at 30 °C, quenched at −100 °C, and heated 0.5 °C/min.

SAXS and WAXS measurements were carried out using a sealed-tube-based pinhole camera. The radiation (Cu $K\alpha$, $\lambda = 1.54$ Å) was monochromatized with multilayer mirrors (Montel Optics by Incoatec), whereafter a double-bounced beam was selected with slits and collimated to the size 0.5 mm × 0.5 mm. The scattering patterns were measured using a HI-STAR multiwire proportional counter (Bruker AXS). The sample detector distance was 170 mm and the covered q range from 0.05 to 1.3 $Å^{-1}$. The transmitted flux was monitored during the measurement through the transparent beam stop, a 3-mm disk press-cut from 0.25-mm-thick copper foil. The samples were measured in flat sample holders with 1 mm path length and 6-μm-thick Mylar windows [40]. The temperature was controlled using a Linkam TP93 hot stage and liquid nitrogen. The background depends on the temperature and was subtracted for each temperature separately. The intensity was normalized to electron scattering units per unit volume using water as a primary standard. $I(0)$ is 0.208 electrons/$Å^3$ for water.

D. Differential scanning calorimetry

Differential scanning calorimetry (DSC) provided an additional monitor of the thermal process. DSC measurements were performed using a Perkin-Elmer Pyris 1 DSC under a nitrogen environment. After heating (from 20 °C to 85 °C) the samples were cooled down to −25 °C for 30 min and heated again up to 85 °C. The scanning rate was 5 °C/min and the sample size was ca. 10 mg.

IV. DATA ANALYSIS

A. Analysis of neutron scattering

The SANS patterns were first qualitatively analyzed by comparison of the absolute intensities, the shape of curves, and the determination of the slope. The scattering cross-section data can be approximated by simple power-law dependence as

$$\frac{d\Sigma(q)}{d\Omega} \sim q^{-\alpha}, \tag{11}$$

where the value of α obtained reflects the likely shape of aggregates in the solution on the studied length scale. If the exponent α is 1, this points to rodlike objects. If α is slightly larger than 2, then the particles can be sheetlike. The scattering curves from all samples followed either one of two types of exponential behaviors. These observations allowed a further analysis of the scattering data by applying the indirect Fourier transformation (IFT) method [41] with rodlike and sheetlike shapes of particles. In the IFT analysis the scattering intensities are expressed via the pair distance distribution function.

The scattering intensities of cylindrical particles are related to the pair distance distribution function of the cylindrical cross section, $\tilde{p}_{CS}(r)$, as

$$\frac{d\Sigma(q)}{d\Omega}\frac{1}{c} = \left(\frac{\pi}{q}\right) 2\pi \int_0^\infty \tilde{p}_{CS}(r) J_0(qr) r\, dr = \left(\frac{\pi}{q}\right) I_{CS}(q), \tag{12}$$

where J_0 is the zeroth-order Bessel function and $I_{CS}(q)$ is the cross-sectional scattering intensity.

For sheetlike particles the scattering intensity is related to the pair distance distribution function of thickness, $\tilde{p}_T(r)$, as

$$\frac{d\Sigma(q)}{d\Omega}\frac{1}{c} = \left(\frac{2\pi}{q^2}\right)\pi \int_0^\infty \tilde{p}_T(r)\cos(qr)dr = \left(\frac{2\pi}{q^2}\right) I_T(q), \tag{13}$$

where $I_T(q)$ is the thickness scattering function.

From the pair distance distribution functions, the mass of aggregates (mass per unit length or unit area) and the radius of gyration can be obtained. The latter is associated with the distribution of scattering length density and with certain assumptions this distribution can be transformed to thickness (T) or radius of cross section (R_{CS}).

B. Analysis of x-ray scattering

The clear-cut data allowed us to use idealized models for SAXS as described in Ref. [42]. As a starting point, we describe the dissolved hairy-rod polymers and the sheets as stiff cylinders. Their scattering intensity is given as

$$I(q,\theta) = \left[2\frac{J_1(qR\sin\theta)}{qR\sin\theta} j_0\left(\frac{qL\cos\theta}{2}\right)\right]^2, \quad (14)$$

where θ is the angle between the q vector and cylinder axis. L is the length and R the radius of the cylinder. The two Bessel functions in Eq. (13) are defined as

$$J_1(x) = \frac{1}{2\pi}\int_0^{2\pi} \exp[i(x\sin\theta - \theta)]d\theta \quad (15)$$

and

$$j_0(x) = \frac{\sin x}{x}. \quad (16)$$

The angular-averaged scattering intensity is obtained by numerical integration over θ. For the rodlike polymers ($R \ll L$) the scattering curve $I(q)$ follows the power law $I(q) \sim q^{-1}$ for $1/L < q < 1/R$. This slope levels off at low angles $q < L^{-1}$ to the Guinier-law regime, whereas at $q > R^{-1}$ it has a downturn corresponding to the cross-sectional scattering $qI(q) \sim \exp(-q^2R^2/4)$ and, finally, to the Porod slope $I(q) \sim q^{-4}$. Similar arguments can be used for sheetlike particles with relative magnitudes of R and L interchanged. In this case the intermediate slope $\sim q^{-2}$ is obtained for $1/R < q < 1/L$.

For these anisotropic extremities the essential form of the intensities may be reduced to the Ornstein-Zernike-type scattering factors [23] as

$$S(q) = \frac{1}{1 + qL\exp(q^2R^2/4)} \quad (17)$$

for the rods and

$$S(q) = \frac{1}{1 + (qR)^2\exp(q^2L^2/12)} \quad (18)$$

for the sheets. In these equations L and R, respectively, indicate the upper limit of validities where the particles still can be regarded as individual rods or sheets.

Of interest here is the power-law behavior $I(q) \sim q^{-1}$ or $\sim q^{-2}$. It can be shown [43] that the intensities from a single particle take, respectively, the form

$$I_1(q) = LA^2(\Delta\rho)^2\frac{\pi}{q} = Z_{\text{tot}}^2\frac{\pi}{qL} \quad (19)$$

for the rods and

$$I_1(q) = AL^2(\Delta\rho)^2\frac{2\pi}{q^2} = Z_{\text{tot}}^2\frac{2\pi}{q^2A} \quad (20)$$

for the sheets. A is the area of the cross section, $\Delta\rho$ the scattering contrast, and Z_{tot} the effective number of scattering electrons in the chain as a whole.

Next we calculate the volume of the normalized intensity for hairy rods dissolved to concentration c (expressed in mass/volume) as

TABLE I. Parameters for linear side-chain PFs: ρ is density, ρ_e electron density, M_l molar mass per unit volume, and ρ_l scattering amplitude per unit length in MCH solvent. The concentration is 10 mg/ml.

Material	ρ (e/Å^3)	ρ_e (e/Å^3)	M_l (g/mol Å)	ρ_l (e/Å^3)
PF6	1.054	0.348	40.0	5.22
PF7	1.035	0.343	43.4	5.42
PF8	1.020	0.339	46.7	5.61
PF9	1.007	0.335	50.1	5.81
PF10	0.996	0.332	53.5	6.01
MCH	0.77	0.265	n/a	n/a

$$i(q) = nI_1(q), \quad (21)$$

where $n = cN_A\rho_l^2/M_l$ is the number density. The intensities are proportional to concentrations and depend on the specific properties of polymers through

$$qi(q) = c\pi N_A\rho_l^2/M_l \quad (22)$$

for the rods and

$$q^2i(q) = c2\pi N_A\rho_s^2/M_s \quad (23)$$

for the sheets. Here M_l and ρ_l are, respectively, the molar mass and scattering amplitude (number of electrons) per unit length whereas M_A and ρ_A are the molar mass and scattering amplitude per unit area. The asymptotic forms of Eqs. (22) and (23) do not depend explicitly on the length of rods or the size of sheets and are valid even for flexible polymers or sheets. When the rods are assumed to be single-polymer chains M_l and ρ_l can be estimated from the bulk properties of polymer and solvent. The values calculated in that way for PFn/MCH systems are given in Table I.

If the polymers self-organize (e.g., in sheetlike membranes) further assumptions concerning the packing density are needed. The density can be calculated in a converse fashion as the properties of single polymers are known. As discussed in the Sec. II, we presume a transition of rods into sheetlike membranes. Let d_s be the average lateral distance of the polymers in the sheets, and assume that the other factors remain constant; we obtain $\rho_s = \rho_l/d_s$ and $M_s = M_l/d_s$. The ratio of two asymptotes is then

$$\frac{\lim_{q\to 0} q^2 i_{\text{sheet}}}{\lim_{q\to 0} qi_{\text{rod}}} = \frac{2}{d_s}. \quad (24)$$

In other words, the crossover point of the intensity curves i_{sheet} and i_{rod} at $q = 2/d_s$ gives an estimate of the packing density d_s, provided that this point is in the power-law region $q < 1/R, 1/L$. Otherwise, the Gaussian correction $\exp[q^2(3R^2 - L^2)/12]$ is necessary. As the phase transition takes place as a function of temperature, the change in the scattering contrast has to be corrected with regard to temperature. However, inasmuch as we are dealing with two distinct phases that yield the same intensity per unit mass at the special point, a total transition between the phases is not

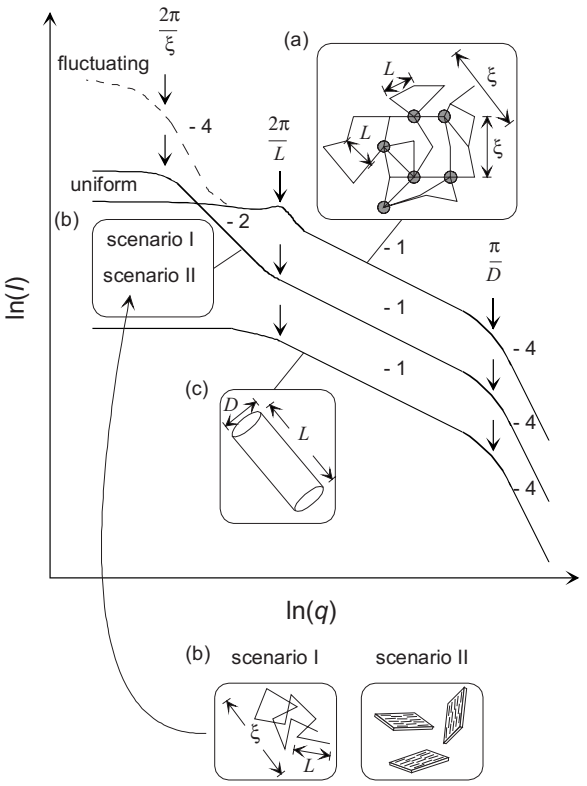

FIG. 4. An idealized description of the small-angle scattering data and proposed solution structures of hairy-rod PFs. (a) A networklike structure with cross-linked nodes. At low q, the solid and dashed lines, respectively, are referred to a uniform network and the network with long-range fluctuations. (b) A structure of rodlike particles forming either Gaussian coils (scenario I) or sheetlike membranes (scenario II) in longer length scales. (c) A structure of fully dissolved rodlike particles (essentially single-polymer chains).

essential, in analogy with the isobastic point known in spectroscopy.

A polymer in dilute solution may also show a crossover from rodlike form to Gaussian (random walk) form for which the scattering scales as q^{-2} for $q<2\pi/\xi$, where ξ is the Kuhn segment. A polymer in a dense solution or gel may contain large-scale density fluctuations which result in a q^{-4} upturn at small angles. These alternatives should be easily distinguished from the above forms by considering where the particular power-law regimens appear in comparison with the experimental data of the structures.

The overall idea of scattering powers is illustrated in Fig. 4. While a mixture of rods and sheets might be mistaken as Gaussian coils, for example, the crossover point between −2 and −1 behavior should occur at very low angles and an extensive −2 region at very low concentration due to the scarcity of such random walk chains. In the present work the clear-cut thermal behavior alone will refute the notion of Gaussian coils.

V. RESULTS AND DISCUSSION

A. Solution structure as a function of side-chain length

The influence of the side-chain length on the solution structure of linear side-chain PFs in MCH has been described in our previous work [14]. In general terms PF6, PF7, PF8, and PF9 were found to form sheetlike aggregates in MCH whereas PF10 dissolves down to the molecular level. These sheets show an odd-even effect so that PF7/MCH and PF9/MCH sheets are thicker but laterally smaller than those of PF6/MCH and PF8/MCH. We have also shown that the internal details of the sheets depend on the side-chain length in a complicated manner. In brief, relatively sharp reflections at $q=0.60$ Å^{-1}, $q=0.48$ Å^{-1}, and $q=0.43$ Å^{-1}, respectively, are seen for PF6/MCH, PF8/MCH, and PF9/MCH with accompanying peaks at the wide angles. Moreover, PF7/MCH, PF8/MCH, and PF9/MCH contain a conformational isomer C_β [14]. This picture is, however, limited to room temperature. Hereafter, the intermolecular nanometer-scale assemblies are presented in a wide temperature range.

Figures 5 and 6, respectively, show examples of SAXS data of PF/MCH mixtures with odd- and even-numbered side chains as a function of temperature. At room temperature, the data show similar solution structures as reported earlier [14]. A sharp visual transition from gel to liquid is seen when heating them from −25 °C to 85 °C. This transition corresponds to the sudden change in the SAXS data essentially from −2 decay to −1 decay. This alteration indicates the structural order-disorder transition from sheetlike structures to fully dissolved rodlike chains. In Fig. 7 we plot characteristic SAXS and WAXS curves for all systems below and above the order-disorder transition. An exception is PF6/MCH, which shows a −2 decay, but no clear phase transition. Moreover, it is likely that the PF6/MCH system is to certain extent macrophase separated as indicated by strong light scattering discussed in Ref. [14]. In this rather high concentration its solution structure is interpreted as lyotropic liquid crystal and surplus solvent. We interpret that the observed lyotropic-sheet and sheet-isotropic phase transitions are equivalent to the lyotropic-membrane and membrane-isotropic phase transitions and N^* and T^*_{mem} concepts introduced in the theoretical section. We may not determine the experimental lyotropic-isotropic phase transition or T^*_{IN} for $N=6$ because the boiling point of the solvent is reached first. However, we expect that the isotropic phase may be achieved with another solvent. These findings constitute the first principle of the phase behavior of PF/MCH system. Still various further details can be discerned.

When considering Figs. 5 and 6, the length of the polymer is not seen in the SAXS data, but the downturn at low angles is likely due to the concentration effects (polymer-polymer interference) and/or the onset of larger-scale morphology (e.g., cross-links or branching). The wider angles reveal in turn a Bragg reflection at around 0.5 Å^{-1}, its strength and exact location depending on the polymer. This maximum refers to the mesomorphic β phase, which is known for solid-state PF8 [26] and PF6 [44]. In Fig. 7 the β reflection 200 [14] is visible to varying degree. The radii of the rods and thicknesses of the sheets as determined by SAXS and WAXS data are compiled in Table II. It is conspicuous that the sheet thicknesses listed in Table II are equivalent to the thickness of two polymer layers, which justifies the idea of a double-layer membrane, an assumption made in Sec. II. Therefore, the sheetlike aggregates discussed are denoted as membranes from this point on.

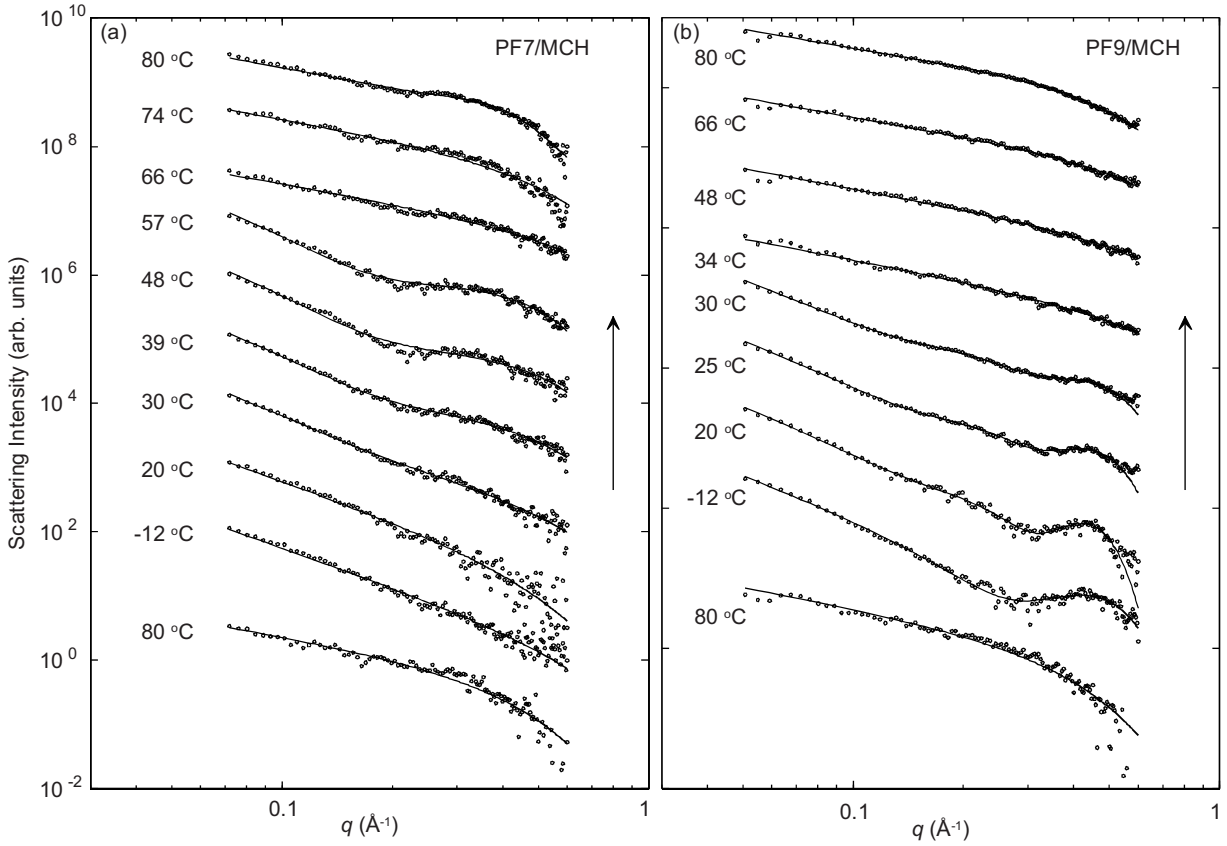

FIG. 5. Open circles present selected SAXS data of PF7/MCH (a) and PF9/MCH (b) during a slow heating (0.1 °C/min) after a heating-cooling cycle from 80 °C to −12 °C. Solid lines correspond to the model described in Sec. IV augmented by a single reflection at a fixed position for PF9/MCH. For PF7/MCH curves corresponding temperatures below 60 °C follow a q^{-2} slope whereas this is true for PF9/MCH below 31 °C. The concentrations were 10 mg/ml.

According to Fig. 7 the change in intensities at the membrane-isotropic transition is similar for all N regardless of T^*_{mem}. Thus the crossing point stays at the same value (also in SANS; cf. Fig. 10 below), which indicates structural similarities in the assembly of the membranes and also points to the fact that essentially the two phases, membranes, and isotropic rods are dominant while the β is a minor component. PF7/MCH and PF9/MCH show a smaller value for the crossing point than the even-numbered side chains, which might be related to looser membrane structure (large d_s; cf. Table II) or, alternatively, thicker membranes (see the scenario in Ref. [14]).

Figure 8 presents the scattering intensities related to the three phases observed in the membrane state of PF8/MCH on slow heating. Figure 9 plots the intensities of loose membranes for all polyfluorenes studied. The values mirror relative abundances of each materials types and should not be taken as exact numbers. The following conclusions can be made. As expected, the contribution from dissolved rods is almost negligible in the membrane phase and increases sharply at T^*_{mem}. The amount of the β phase of PF8 decreases sharply at T^*_{mem}. This transition has a phenomenological counterpart in the disappearance of the conformational isomer C_β in dilute PF8/MCH mixtures [10]. Finally, the scattering power of loose membranes increases with temperature in all cases until the sudden drop at T^*_{mem}. Besides the contrast increase this might also imply that for $T<T^*_{\mathrm{mem}}$ the tendency for membrane formation becomes stronger with temperature until the membrane-isotropic phase transition. This observation is commensurate with the theoretical assumption of stable membranes for the interval $T^*_{IN}<T<T^*_{\mathrm{mem}}$ and metastable membranes for $T<T^*_{IN}$; cf. Fig. 2.

The isotropic solution demixes at a certain temperature. The appearance of the membranes can be connected to the narrow interval where the membranes are suggested to be stable (as shown in Fig. 2). Upon lowering the temperature the system tends to demix, but this occurs very slowly due to the network of membranes (as proposed for PF/MCH in Ref. [14]). Alternatively, membrane formation can be hypothesized for purely kinetic reasons. In a such case there would be no T^*_{mem} and the solution demixes at T^*_{IN}, but hairy-rods form membrane "precursors" that get arrested due to the gelation. However, the first explanation seems plausible to us. When the solution demixes, the polymers prefer maximal contact to protect them from the solvent, which would not be manifested by two-dimensional but three-dimensional precursors.

B. Solution structure as a function of side-chain branching

As the case $N=8$ represents a magic number when maximizing the amount of C_β isomer in the PF/MCH system [14],

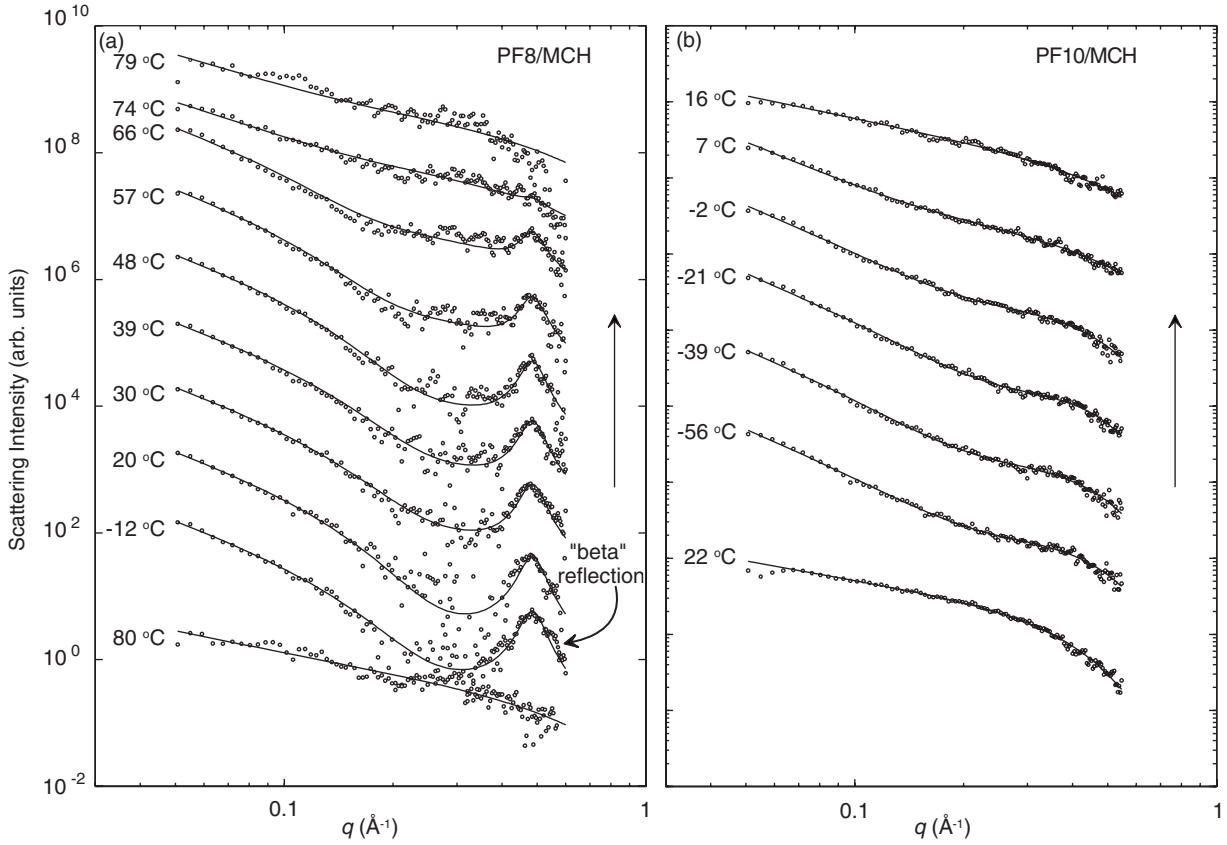

FIG. 6. Open circles present selected SAXS data of PF8/MCH (a) and PF10/MCH (b) during a slow heating (0.1 °C/min) after a heating-cooling cycle from 80 °C to −12 °C. Solid lines correspond to the model described in Sec. IV augmented by a single reflection at a fixed position for PF8/MCH. A distinctive "β" maximum is present for PF8/MCH at 0.46 Å^{-1}. The concentrations were 10 mg/ml.

it deserves more attention. We have previously shown that while PF8/MCH organizes into sheetlike assemblies (henceforth membranes) at room temperature, the system composed by a branched side-chain PF2/6 forms only an isotropic phase [13]. PF2/6 and PF8 have the same amount of side-chain beads, the side chains differing only in terms of branching (cf. Fig. 3). The other factors influencing phase behavior are constant. In order to study the solution structure as a function of side-chain branching for $N=8$ further, we synthesized F2/6-F8 random copolymers and varied the fraction of F8 and F2/6 monomers from one extreme to another (see Sec. III).

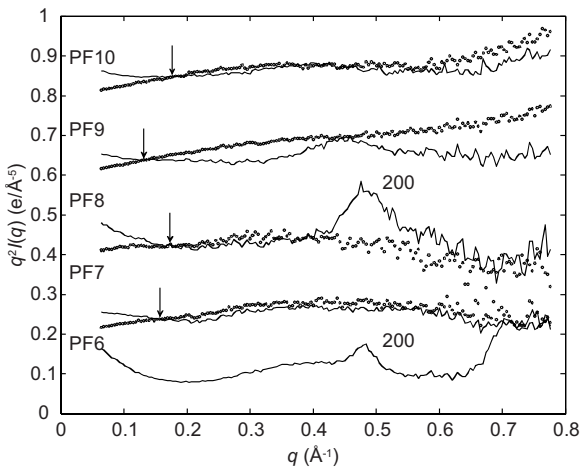

FIG. 7. The SAXS/WAXS data multiplied by q^2 of linear side-chain PF/MCH mixtures. Solid lines represent the situation below and dotted lines above the membrane-isotropic phase transition. The arrows mark the crossing points of −1 and −2 slopes.

F2/6$_{0.95}$-fluorenone$_{0.05}$ polymer mixed in MCH was studied for comparison. The motivation for this stems from the fact that 9-fluorenone repeat units represent keto defects arising from PF oxidation [18,45]. This latter experiment thus mirrors whether 5% oxidation influences the PF2/6 solution structure in MCH. The synthesized copolymer represents se-

TABLE II. Various parameters characterizing the thicknesses of the sheets of linear side-chain PFs in 10 mg/ml MCH as determined by SAXS and WAXS. The radius of the rod (R) has been obtained from fitting Eq. (17). The thicknesses of the sheets (d_β and d_s) are calculated, respectively, from the sharp "β" maximum and from the crossing point of the data. The concentrations were 10 mg/ml.

Polymer in MCH	R(Å)	d_β(Å)	d_s(Å)
PF6	n/a	13.1	n/a
PF7	3.9	n/a	12
PF8	n/a	13.1	11
PF9	3.9	13.7	15
PF10	4.4	n/a	11

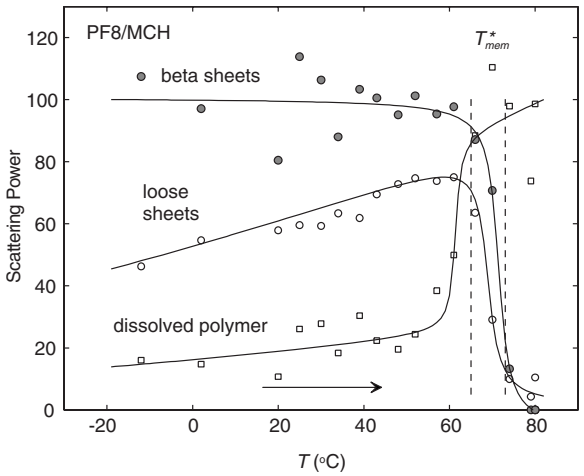

FIG. 8. Observed thermal behavior of the scattering components (intensities) related to the β sheets (solid circles), loose sheetlike membranes (open circles), and dissolved rodlike polymers (open squares) in a 10 mg/ml PF8/MCH system. The intensities are scaled to 100 by extrapolation the transition temperature, supposing a total transition. The order-disorder transition is marked by vertical dotted lines. The β phase is located within the membranes and can be distinguished from the loose membrane by a Bragg reflection.

rious oxidation, because already the 0.1% oxidation level is optically pronounced [45]. Therefore, if the solution structure of F2/6$_{0.95}$-fluorenone$_{0.05}$ corresponded to that of PF2/6, the structure of any slightly oxidated PF2/6 would do the same.

On the mixing and heating-cooling cycle F8$_{0.95}$-F2/6$_{0.05}$/MCH-d_{14} and F8$_{0.90}$-F2/6$_{0.10}$/MCH-d_{14} form viscous gels resembling PF8/MCH, whereas F8$_{0.50}$-F2/6$_{0.50}$/MCH-d_{14} and F2/6$_{0.95}$-fluorenone$_{0.05}$/MCH-d_{14} remain transparent liquids akin to PF2/6/MCH. Figure 10 plots SANS data of the copolymers studied after the heating-cooling cycle at 20 °C. The data of F8$_{0.95}$-F2/6$_{0.05}$/MCH-d_{14} and F8$_{0.90}$-F2/6$_{0.10}$/MCH-d_{14} differ clearly from those of F8$_{0.50}$-F2/6$_{0.50}$/MCH-d_{14} and

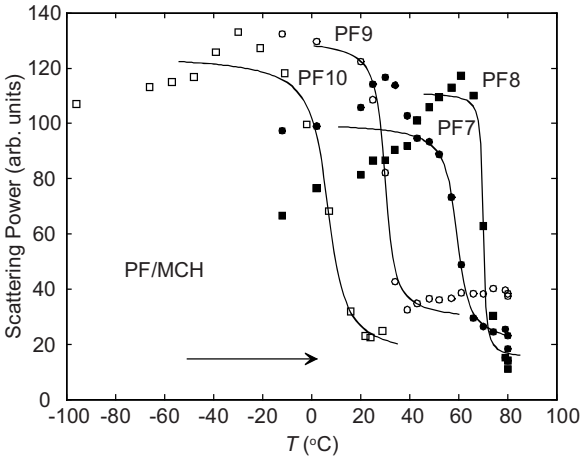

FIG. 9. Scattering power of membrane contribution in the SAXS data of PF7 (solid circles), PF8 (solid squares), PF9 (open circles), and PF10 (open squares) in MCH. The data correspond to those shown in Figs. 5 and 6. Concentrations were 10 mg /ml.

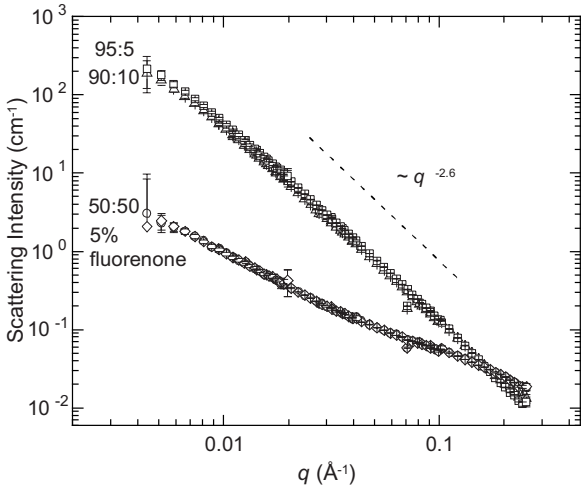

FIG. 10. SANS data of F8$_{0.95}$-F2/6$_{0.05}$ (open squares), F8$_{0.90}$-F2/6$_{0.10}$ (open triangles), F8$_{0.50}$-F2/6$_{0.50}$ (open circles), and F2/6$_{0.95}$-fluorenone$_{0.05}$ (open diamonds) in 10 mg/ml MCH-d_{14} at 20.0 °C ± 0.5. The dashed line shows the −2.6 decay for comparison.

F2/6$_{0.95}$-fluorenone$_{0.05}$/MCH-d_{14}. The former materials show a distinctive −2 decay while the latter ones follow a −1 slope. These observations point to membrane and isotropic phases like those of PF8/MCH and PF2/6/MCH. This means that any difference between the solution structure of F8$_{0.90}$-F2/6$_{0.10}$/MCH-d_{14} and PF8/MCH is subtle. The keto defects as illustrated by F2/6$_{0.95}$-fluorenone$_{0.05}$ are not found to play a role either. Note that the intensity curves in Fig. 10 cross at high q, which implies that most of the material must be in one single phase.

When the F8$_{0.95}$-F2/6$_{0.05}$/MCH-d_{14} and F8$_{0.90}$-F2/6$_{0.10}$/MCH-d_{14} mixtures showing the existence of two-dimensional structure at room temperature are heated (up to 84 °C), they undergo a visual phase transition to transparent fluid. The obvious question is, then, whether this affects the structure in the same way as in PF8/MCH-d_{14}. Figure 11 plots SANS data of these samples at 84 °C. The corresponding data of PF8/MCH-d_{14} are shown for comparison. All data confirm a distinctive −1 decay, indicating a phase transition from the proposed membrane phase to the fully dissolved hairy-rods (cf. Fig. 1). These clear-cut characteristics allowed us to fit the data to models of cylindrical or sheetlike particles. The essential structural parameters so obtained are compiled in Table III. The thicknesses of sheets correspond to two-polymer layers. Thus, the experimental data are in agreement with the notation and theory of a double-layer membrane.

C. Phase diagram

The exact transition temperature T^*_{mem} was studied for all the above-mentioned systems in detail by SAXS and DSC. Representative examples of DSC data are plotted in Fig. 12. The distinct peaks are interpreted as membrane-isotropic phase transitions representing the transition temperature T^*_{mem}. These values correspond well to those determined by

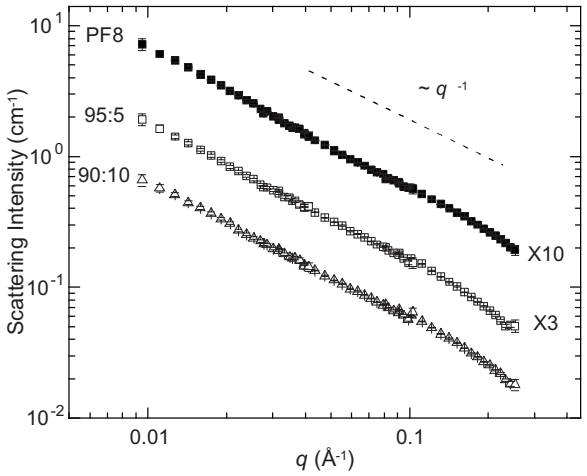

FIG. 11. SANS data of PF8 (solid squares), $F8_{0.95}$-F2/$6_{0.05}$ (open squares), and $F8_{0.90}$-F2/$6_{0.10}$ (open triangles) in MCH-d_{14} at 84 °C ± 1. The two latter data are shifted for clarity. The dashed line shows the −1 decay for comparison. The concentrations were 10 mg/ml.

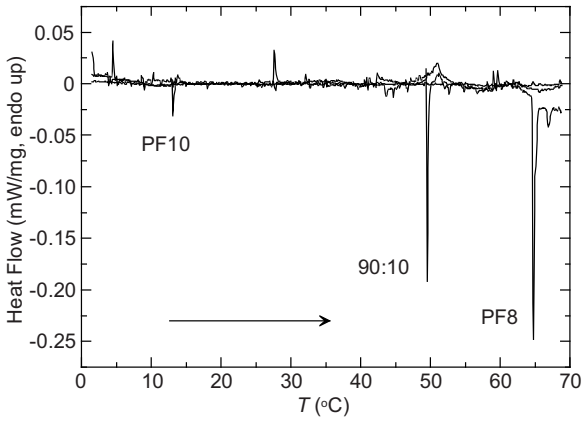

FIG. 12. The DSC data of PF10, $F8_{0.90}$-F2/$6_{0.10}$ copolymer, and PF8 in 10 mg/ml MCH during heating (5 °C/min) after a heating-cooling cycle (from 85 °C to −25 °C). The distinct peaks are interpreted as membrane-isotropic phase transitions representing the transition temperature T^*_{mem}.

SAXS. The observed membrane-isotropic transitions are compiled in Table IV.

Figure 13 plots the proposed experimental phase diagram providing a comparison to the theoretical phase diagram shown in Fig. 2. In the Sec. II we predict an intermediate membrane phase of a hairy-rod solution, and this is indeed experimentally confirmed. Importantly, the theoretically predicted scaling of T^*_{mem} illustrated in Fig. 2 is in accordance with the experimental data for $N \geq 8$ presented in Fig. 13. Several issues should be moreover commented on.

First, although the equations shown in Sec. II are interpreted as semiquantitative rather than exact, the physics behind the solution-to-membrane transition is easily reasoned. Apparently, the free energy of the system includes two major contributions. The first one—the elastic energy of the "blurs" formed by the alkyl chains—is mainly of entropic origin. The other—the interaction between rods and a poor (for the backbones) solvent—has a significant enthalpic component. This means that at high temperatures when the entropy is dominating, the state with the lower stretching should be more advantageous. The hairy rods are thus dissolved in the solvent because the elastic energy of the side chains of such a cylindrical brush is apparently lower than that of a planar one (cf. Fig. 1). Lowering the temperature amplifies the enthalpic term responsible for the solvent-backbone interaction. Hence, at a certain point the system strives to reduce the backbone-solvent contact area in spite of the higher stretching of the side chains and membranes are formed. Upon further cooling the system macroscopically demixes in line with earlier predictions [22]. It is expected that analogous *n*-alkanes are dissolved in MCH [46]. The question is whether T^*_{mem} is related to their melting temperature, which increases with increasing N [47]. We may argue that the dissolution and melting of the side chains are entropically inverse phenomena and therefore the opposite behavior seems logical.

Second, both scattering and DSC data point to the prominent decrease of T^*_{mem} with increasing number of side-chain beads. Although not directly included in the model, a two-branched side chain having N side-chain beads can be roughly seen as two $N/2$ chains with twice as high grafting density—i.e., a distance $b/2$ between the grafts. As follows from Eq. (8), $T^*_{mem} \sim b^{5/3}/N$ decreases in such a case. This qualitatively corresponds to the experimentally observed decrease of T^*_{mem} with side-chain branching.

Third, the samples in the membrane phase are metastable, a slow macrophase separation occurring a few days after preparation. This separation is slow enough not to infer the

TABLE III. Various parameters characterizing the structures of PF copolymers in 10 mg/ml MCH-d_{14} as determined by SANS: D is the maximal size of the homogeneous cross section, $R_{CS,g}$ the cross-sectional radius of gyration, and $R_{T,g}$ the radius of gyration of thickness.

Polymer in MCH-d_{14}	Temperature (°C)	Model	Analyzed q range (Å)	D_{max} (Å)	$R_{CS,g}$ (Å)	$R_{T,g}$ (Å)
$F8_{0.50}$-F2/$6_{0.50}$	20.0 ± 0.5	Cylinder	0.03–0.3	~50	12.8 ± 0.6	n/a
$F8_{0.90}$-F2/$6_{0.10}$	20.0 ± 0.5	Sheet	0.004–0.3	~30	n/a	8.8 ± 0.2
$F8_{0.95}$-F2/$6_{0.05}$	20.0 ± 0.5	Sheet	0.004–0.3	~30	n/a	8.7 ± 0.2
$F8_{0.90}$-F2/$6_{0.10}$	84 ± 1	Cylinder	0.03–0.3	~50	11.0 ± 0.7	n/a
$F8_{0.95}$-F2/$6_{0.05}$	84 ± 1	Cylinder	0.03–0.3	~50	11.1 ± 0.7	n/a
PF8	84 ± 1	Cylinder	0.03–0.3	~50	13.1 ± 0.6	n/a

TABLE IV. Transition temperature (T^*_{mem}) for the membrane-isotropic phase transition of the PF samples in 10 mg/ml MCH as determined by DSC and SAXS.

Polymer in MCH	DSC	SAXS
	T^*_{mem} (°C)	T^*_{mem} (°C)
PF6	n/a	n/a
PF7	Not observed	59 ± 4
PF8	65 ± 2	70 ± 1
PF9	Not observed	30 ± 3
PF10	13 ± 2	7 ± 5
$F8_{0.95}$-F2/$6_{0.05}$	56 ± 4	56 ± 5
$F8_{0.90}$-F2/$6_{0.10}$	50 ± 2	48 ± 6
$F8_{0.50}$-F2/$6_{0.50}$	Not observed	Not observed

measurements. We expect that for the long side chains the membranes can survive for long times even in the phase regime where demixing should have taken place. The free energy difference between membranes and the macrophase-separated system is quite low and, if membranes are interconnected (as is expected in Ref. [14]), their restricted mobility will considerably slow down the process. The polymer demixing transition T^*_{IN} is not marked in the experimental phase diagram, but this does not mean that it would not take place in experiment. Interestingly, the β phase is generally understood as an intrinsically metastable, an intermediate state between a solvent-induced clathrate and the crystalline order of the undiluted state [26]. The metastability in the solid state is in this respect in agreement with the proposed theoretical model and with the experimental data of the proposed β phase in PF/MCH mixtures.

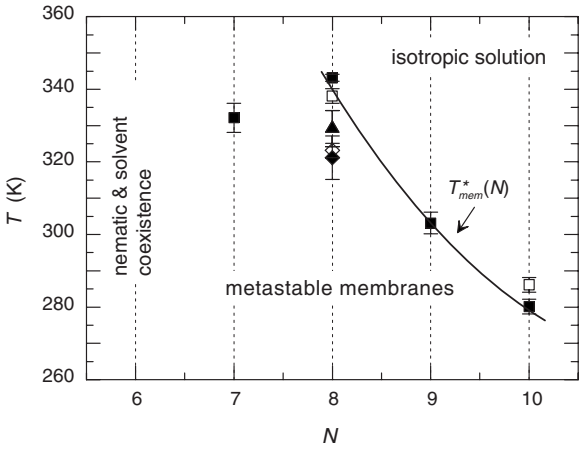

FIG. 13. The experimental phase diagram of PFs showing the membrane-isotropic phase transition temperature T^*_{mem} as a function of side-chain beads, N. The data are based on SAXS (solid squares) and DSC (open squares) measurements. Also shown are corresponding transitions $T^*_{mem}(N=8)$ for $F8_{0.95}$-F2/$6_{0.05}$ (triangles) and $F8_{0.90}$-F2/$6_{0.10}$ (diamonds) random copolymers. These have been derived from the SAXS (solid symbols) and DSC (open symbols) measurements. The dotted lines correspond to the experimentally studied N. The solid line separating two phase regimes is a guide to the eye. The theoretical counterpart of this phase diagram is shown in Fig. 2.

Fourth, in the theory [Eq. (1)] the interaction between the hairy rods is neglected, which is a plausible assumption in a low-concentration regime. The concentration used ($\sim$1 wt %) constitutes an uncorrelated particle system and no concentration effect is seen, when the concentration is lowered down to 5 mg/ml [13]. However, as shown elsewhere [23], the PF aggregates are able to form larger, networklike structures. We have in addition proposed that the "β" crystallites act as nodes of such a network, which implies that the membranes are interconnected [14]. Thus, a negligible interaction assumption certainly holds for the isotropic phase, but should be considered with care otherwise.

We do not make conclusions on the kinetics in the present study, but note that the gelation transitions are well-known for *n*-alkanes [48] and, for instance, for poly(methyl methacrylate) in toluene [49]. The latter system shows a two-step thermoreversible gelation mechanism where a fast intramolecular conformational change is followed by an intermolecular association.

We finally note that we were able to determine the phase transitions for all membrane systems by SAXS, but not by DSC (Table IV). The transitions in PF7 and PF9 membranes were not manifested by significant heat flow in the DSC curves. Whether this fact relates to the odd-even sequence in the internal structure of the sheets [14] remains an open question.

VI. CONCLUSIONS

In conclusion, we have conducted a systematic study on how the phase behavior of PFs can be controlled by the side-chain length and branching. The experimental work was grounded on the theoretical framework and good qualitative agreement was found. PF6, PF7, PF8, PF9, PF10, and F8-F2/6 random copolymers were employed as model polymers and MCH used as a representative solvent. The lyotropic phase with solvent coexistence as well as the membrane phase and isotropic phase of dissolved rodlike polymers were found. At lower temperatures, the lyotropic and membrane phases occur with increasing number of side-chain beads, N, the phase transition being at $N^* \sim 6$. The membrane phase turns into the isotropic phase when the temperature is increased up to the limit $T^*_{mem}(N)$. This transition temperature T^*_{mem} decreases with N ($>N^*$) and with the degree of side-chain branching. In theory, this picture is complemented by polymer demixing with the transition temperature $T^*_{IN}(N)$, its value decreasing with N. In experiment, the membrane phase was found to consist of loose sheets of two-polymer layers, laterally better packed β phase and also fully dissolved polymers. For $N \geq 7$ and $T < T^*_{mem}$ the tendency for membrane formation becomes stronger with increasing temperature. This observation is in phenomenological accordance with the theory which assumes stable membranes for the interval $T^*_{IN} < T < T^*_{mem}$ and membrane nematic coexistence for $T < T^*_{IN}$. Besides these principles of phase behavior, a quantitative presentation of the structural parameters has been given. These results form a solid insight when tailoring solution assemblies of hairy-rod polyfluorenes.

ACKNOWLEDGMENTS

We thank F. B. Dias of the University of Durham, L. Almásy of the Budapest Neutron Centre, H. D. Burrows of the University of Coimbra, and M. J. Winokur of the University of Wisconsin for discussions. SANS experiments were supported by the European Commission, the 6th Framework Program through the Key Action: Strengthening the European Research Area, Research Infrastructures (Contract No. RII3-CT-2003-505925). Thanks are also due to W. D. Carswell of the University of Durham for access to the thermal analysis.

[1] P.-G. de Gennes, *Scaling Concepts in Polymer Physics* (Cornell University Press, Ithaca, NY, 1979).
[2] A. Y. Grosberg and A. R. Khokhlov, *Statistical Physics of Macromolecules* (American Institute of Physics, Woodbury, NY, 1994).
[3] G. Wegner, Macromol. Chem. Phys. **204**, 347 (2003).
[4] M. J. Winokur, in *Handbook of Conducting Polymers*, edited by T. A. Skotheim and J. R. Reynolds (CRC Press, Boca Raton, FL, 2007), Vol. 1, p. 1.
[5] A. C. Grimsdale and K. Müllen, Adv. Polym. Sci. **199**, 1 (2006).
[6] M. Knaapila, R. Stepanyan, B. P. Lyons, M. Torkkeli, and A. P. Monkman, Adv. Funct. Mater. **16**, 599 (2006).
[7] D. Neher, Macromol. Rapid Commun. **22**, 1365 (2001).
[8] U. Scherf and E. J. W. List, Adv. Mater. **14**, 477 (2002).
[9] J. Zaumseil and H. Sirringhaus, Chem. Rev. **107**, 1296 (2007).
[10] F. B. Dias, J. Morgado, A. L. Macanita, F. P. da Costa, H. D. Burrows, and A. P. Monkman, Macromolecules **39**, 5854 (2006).
[11] M. Grell, D. D. C. Bradley, X. Long, T. Chamberlain, M. Inbasekaran, E. P. Woo, and M. Soliman, Acta Polym. **49**, 439 (1998).
[12] C. C. Kitts and D. A. Vanden Bout, Polymer **48**, 2322 (2007).
[13] M. Knaapila, V. M. Garamus, F. B. Dias, L. Almásy, F. Galbrecht, A. Charas, J. Morgado, H. D. Burrows, U. Scherf, and A. P. Monkman, Macromolecules **39**, 6505 (2006).
[14] M. Knaapila, F. B. Dias, V. M. Garamus, L. Almásy, M. Torkkeli, K. Leppänen, F. Galbrecht, E. Preis, H. D. Burrows, U. Scherf, and A. P. Monkman, Macromolecules **40**, 9398 (2007).
[15] G. Fytas, H. G. Nothofer, U. Scherf, D. Vlassopoulos, and G. Meier, Macromolecules **35**, 481 (2002).
[16] M. Knaapila, R. Stepanyan, M. Torkkeli, B. P. Lyons, T. P. Ikonen, L. Almásy, J. P. Foreman, R. Serimaa, R. Güntner, U. Scherf, and A. P. Monkman, Phys. Rev. E **71**, 041802 (2005).
[17] E. Somma, B. Loppinet, C. Chi, G. Fytas, and G. Wegner, Phys. Chem. Chem. Phys. **8**, 2773 (2006).
[18] F. B. Dias, M. Knaapila, A. P. Monkman, and H. D. Burrows, Macromolecules **39**, 1598 (2006).
[19] L. Wu, T. Sato, H.-Z. Tang, and M. Fujiki, Macromolecules **37**, 6183 (2004).
[20] M. J. Banach, R. H. Friend, and H. Sirringhaus, Macromolecules **37**, 6079 (2004).
[21] S. Moynihan, D. Iacopino, D. O'Carroll, D. Lovera, and G. Redmond, Chem. Mater. **20**, 996 (2008).
[22] M. Ballauff, Macromolecules **19**, 1366 (1986).
[23] M. H. Rahman, C.-Y. Chen, S.-C. Liao, H.-L. Chen, C.-S. Tsao, J.-H. Chen, J.-L. Liao, V. A. Ivanov, and S.-A. Chen, Macromolecules **40**, 6572 (2007).
[24] M. J. Winokur, J. Slinker, and D. L. Huber, Phys. Rev. B **67**, 184106 (2003).
[25] S. H. Chen, A. C. Su, C. H. Su, and S. A. Chen, Macromolecules **38**, 379 (2005).
[26] S. H. Chen, A. C. Su, and S. A. Chen, J. Phys. Chem. B **109**, 10067 (2005).
[27] M. Arif, C. Volz, and S. Guha, Phys. Rev. Lett. **96**, 025503 (2006).
[28] W. Chunwaschirasiri, B. Tanto, D. L. Huber, and M. J. Winokur, Phys. Rev. Lett. **94**, 107402 (2005).
[29] C. Rothe, S. M. King, F. Dias, and A. P. Monkman, Phys. Rev. B **70**, 195213 (2004).
[30] C. Rothe, F. Galbrecht, U. Scherf, and A. Monkman, Adv. Mater. **18**, 2137 (2006).
[31] J. Teetsov and D. A. Vanden Bout, Langmuir **18**, 897 (2002).
[32] W.-C. Ou-Yang, C.-S. Chang, H.-L. Chen, C.-S. Tsao, K.-Y. Peng, S.-A. Chen, and C. C. Han, Phys. Rev. E **72**, 031802 (2005).
[33] A. Subbotin, M. Saariaho, O. Ikkala, and G. ten Brinke, Macromolecules **33**, 3447 (2000).
[34] R. Stepanyan, A. Subbotin, M. Knaapila, O. Ikkala, and G. ten Brinke, Macromolecules **36**, 3758 (2003).
[35] A. Subbotin, R. Stepanyan, M. Knaapila, O. Ikkala, and G. ten Brinke, Eur. Phys. J. E **12**, 333 (2003).
[36] S. T. Milner, T. A. Witten, and M. E. Cates, Macromolecules **21**, 2610 (1988).
[37] H. Cheun, F. Galbrecht, B. S. Nehls, U. Scherf, and M. J. Winokur, J. Lumin. **122–123**, 212 (2007).
[38] H. B. Stuhrmann, N. Burkhardt, G. Dietrich, R. Jünemann, W. Meerwinck, M. Schmitt, J. Wadzack, R. Willumeit, J. Zhao, and K. H. Nierhaus, Nucl. Instrum. Methods Phys. Res. A **356**, 124 (1995).
[39] G. D. Wignall and F. S. Bates, J. Appl. Crystallogr. **20**, 28 (1987).
[40] K. S. Vahvaselkä, R. Serimaa, and M. Torkkeli, J. Appl. Crystallogr. **28**, 189 (1995).
[41] O. Glatter, J. Appl. Crystallogr. **10**, 415 (1977).
[42] J. S. Pedersen, Adv. Colloid Interface Sci. **70**, 171 (1997).
[43] G. Porod, in *Small Angle X-ray Scattering*, edited by O. Glatter and O. Kratky (Academic Press, London, 1982).
[44] S. H. Chen, A. C. Su, C. H. Su, and S. A. Chen, J. Phys. Chem. B **110**, 4007 (2006).
[45] S. I. Hintschich, C. Rothe, S. Sinha, A. P. Monkman, P. Scandiucci de Freitas, and U. Scherf, J. Chem. Phys. **119**, 12017 (2003).

[46] H. Iloukhani and M. Rezaei-Sameti, J. Mol. Liq. **126**, 62 (2006).
[47] R. Boese, H.-C. Weiss, and D. Bläser, Angew. Chem. Int. Ed. Engl. **38**, 988 (1999).
[48] D. J. Abdallah and R. G. Weiss, Langmuir **16**, 352 (2000).
[49] M. Berghmans, S. Thijs, M. Cornette, H. Berghmans, F. C. De Schryver, P. Moldenaers, and J. Mewis, Macromolecules **27**, 7669 (1994).